REVIEW

Optimizing Reinforcement Strategies for Improved Flexural Behavior in Reinforced Concrete Walls

Ahmed Yahia[1], Magdy Tayel[1], Khalid Heiza[1] and Ghada Hekal[1,2*]

Abstract

This study investigates the flexural behavior of reinforced concrete walls through the testing of eight large-scale cantilever structural wall (CSW) specimens, categorized into two groups with varying steel reinforcement configurations and aspect ratios. The specimens underwent monotonically increasing lateral loading until failure. Key test parameters included the addition of vertical steel reinforcement in boundary elements, vertical steel reinforcement in boundary elements with steel mesh near the foundation, and the incorporation of diagonal embedded columns. A control specimen, reinforced with traditional methods, was also examined. The results demonstrate that different steel reinforcement configurations led to significant increases in both cracking loads (8.3% to 72.86%) and peak loads (5.27% to 54.51%). Notably, specimens reinforced with vertical reinforcement in boundary elements, along with diagonal mesh near the foundation, exhibited the highest peak load increases of 52.71% and 54.51% for aspect ratios of 1.5 and 2.0, respectively. Moreover, the use of vertical steel reinforcement in boundary elements resulted in substantially higher ductility, with increases of 128% and 41.7% for aspect ratios of 1.5 and 2.0, respectively. The study concluded by employing nonlinear 3D finite element analysis in the ABAQUS program to predict the behavior of reinforced concrete shear wall test specimens subjected to a combination of axial and lateral forces, achieving predictions of acceptable accuracy. This research contributes valuable insights to the understanding of reinforced concrete wall behavior, with potential implications for structural design and engineering applications.

Keywords Flexural behavior, Steel reinforcement configurations, Large-scale cantilever structural wall, Peak loads, Nonlinear 3D finite element analysis

1 Introduction

Reinforced concrete (RC) shear walls exhibit exceptional load-bearing capacity and high stiffness, serving as crucial structural elements for carrying axial forces and withstanding lateral forces. However, in comparison to RC frames, RC shear walls often display limited ductility, making them more susceptible to brittle shear failure. Consequently, numerous studies have been undertaken to enhance the deformability and seismic performance of (RC) shear walls through various strengthening techniques. These include reinforcement with carbon fiber-reinforced polymer bars (Huang, et al., 2020; Zhao et al., 2019, Zhao et al., 2019, Huang et al., 2020),incorporation of vertical and inclined steel braces (Zhang et al., 2019, Zhang et al., 2021) (Zhang et al., 2019, 2021), utilization of embedded spiral transverse bars (Hosseini et al., 2022) (Hosseini, Yekrangnia and Vatani Oskouei, 2022), and exploration of (RC) shear walls with diverse aspect ratios (Hosseini et al., 2022; Wei et al., 2022; Zhang,

*Correspondence:
Ghada Hekal
gahda.mousa@sh-eng.menofia.edu.eg
[1] Civil Engineering Department, Menoufia University, Shibin El Kom, Egypt
[2] Department of Civil Engineering, Faculty of Engineering, Menoufia University, Shibin El Kom, Egypt

Yahia *et al. Int J Concr Struct Mater*   (2025) 19:24

Page 2 of 24

et al., 2021, Wei, Chen and Xie, 2022, Zhang et al., 2021). In a comprehensive study, six concrete shear walls were subjected to cyclic loading until failure. Among them, one wall was steel-reinforced concrete (RC), while the remaining five walls were reinforced with CFRP grids, employing two configurations—either vertically or horizontally laid. The specimens featuring CFRP grids demonstrated enhanced shear resistance, evidenced by larger lateral drift, increased load capacity, greater strain, and reduced residual deformation. Notably, walls with horizontally laid CFRP grids exhibited particularly improved performance compared to conventional RC shear walls (Huang, et al., 2020, Huang et al., 2020). A comprehensive study encompassed six shear walls employing high-strength concrete and high-strength steels, incorporating cyclic load tests. The investigation included two reinforced concrete shear walls and four composite walls reinforced by concrete-filled steel tubes (CFSTs). The research findings indicated that specimens reinforced with steel fibers exhibited lighter damage, lower deformation capacity, and a reduced proportion of shear deformation compared to their non-fiber reinforced counterparts (Li, et al., 2023, Li et al., 2023). In separate studies, (Li, et al., 2022; Xing, et al., 2022, Xing et al., 2022, Li et al., 2022) conducted tests on reinforced concrete (RC) shear walls, exploring the impact of diagonal steel bar bracings in the wall web, embedded steel tubes in the boundary zone, and concealed steel truss on seismic behavior. Results revealed that both reinforcement and channel steel bracings restrained crack development, reducing crack widths, with channel steel bracings exhibiting a more pronounced effect in mitigating wall damage. In another investigation, (Zhang, et al., 2021, Zhang et al., 2021) delved into the seismic behavior of steel fiber-reinforced high-strength concrete shear walls with different embedded steel configurations. The study involved five half-scale shear walls, including four conventional reinforced concrete walls and one composite wall. Results highlighted the significance of HRB 600 MPa reinforcement in the boundary element and wall web for improved seismic performance. Furthermore, (Nagib, et al., 2022, Nagib et al., 2022)explored the effect of bond properties between ultra-high performance fiber-reinforced concrete (UHPFRC) layers and normal strength concrete (NSC) on the performance of strengthened composite squat shear walls through shear cyclic tests. Findings emphasized the impact of concrete substrate surface roughness, shear connectors usage, and UHPFRC layers thickness on shear bond behavior. The installation of shear connectors significantly enhanced post-peak shear behavior, altering the failure mode from brittle to ductile. Additionally, (Du et al., 2020, Du, Luo and Sun, 2020) conducted an experimental study on the

moment–shear force interaction's effect on the seismic performance of shear walls. The study involved three identical 2-story shear wall specimens representing the lower portion of an 11-story high-rise building. Results demonstrated the significant influence of moment–shear force interaction on failure patterns, hysteretic characteristics, ductility, and energy dissipation. Moreover, (Ren, et al., 2022, Ren et al., 2022) carried out an experimental and finite element analysis using glass fiber-reinforced polymer (GFRP) tubes to reinforce concrete-filled multicellular steel tubular (CF-MCST) shear walls under cyclic loads. Findings indicated that GFRP-tube reinforced CF-MCST shear walls yielded upon the steel tube's ultimate tensile strength and local concrete crushing. Several other studies (Barros Silva et al., 2023; Hasan et al., 2023; Hu et al., 2023, Hu, Fang and Benmokrane, 2023, Hasan, Qasem and Muhamad, 2023, de Barros Silva, Horowitz and Bernardo, 2023) utilized finite element analysis to compare experimental and numerical results, examining load–displacement responses, stiffness degradation, and modes of failure. For instance, (Hu et al., 2023, Hu, Fang and Benmokrane, 2023) focused on the cyclic behavior of ultra-high-performance concrete (UHPC) shear walls with hybrid reinforcement of fiber-reinforced polymer (FRP) and steel bars. The numerical model, employing the concrete damage plasticity (CDP) model in ABAQUS, demonstrated an acceptable level of accuracy in predicting the cyclic behavior observed in the six UHPC shear walls experimentally tested.

Excessive reliance on shear walls for both vertical and horizontal lateral resistance in high-rise buildings often leads to thicker shear walls at the base, restricting usable space within the structure. To address this limitation and ensure sufficient deformation capacity, the current study was conducted to investigate the flexural performance of shear walls with varying aspect ratios under static horizontal loading until failure. The main principle for comparison between studied specimens based on improving the flexural behavior of concrete shear walls reinforced with different reinforcement strategies with constant steel reinforcement ratios for longitudinal steel bars which directly influence in flexural resistance. Therefore, it is noted that the steel reinforcement ratios in the first three specimens from each group were constant with 6T12 per side. Specimen RW1 reinforced with traditional reinforcement method, while in specimen RW2 the same number of vertical reinforcing steel bars was used, but in another mechanism, which is creating embedded columns at concentration stresses zones. Specimen RW3 typically reinforced as specimen RW2 was added mesh reinforcement in the last third of the wall as a development for sample No. 2. Finally, specimen RW4 reinforced only with 5T10 per side, because the embedded inclined

Yahia *et al. Int J Concr Struct Mater*   (2025) 19:24

Page 3 of 24

column reinforced with 4T12 has a great effect in transmitting the lateral forces acting on the shear walls and transferring them from the point of loading to the foundations directly in the terms of axial forces, whether tensile or compressive, depending on the direction of loading which lead to increase wall load capacity, therefore inclined embedded column reinforcement taken into account within the vertical steel reinforcement ratios by 50%. In contrast to previous research, which used constant longitudinal reinforcement bar ratios in addition of diagonal bars as embedded column. The objectives of the research are twofold: first, to examine the impact of different aspect ratios on reinforced concrete shear walls; and second, to assess the flexural behavior, energy absorption, and ductility of concrete shear walls reinforced with alternative steel configurations compared to traditional reinforcement methods.

2 Experimental program

2.1 Specimen design

A series of eight large-scale cantilever structural wall (CSW) specimens, all possessing identical dimensions but featuring distinct steel reinforcement configurations (see Figs. 1, 2, 3), underwent testing under monotonically increasing lateral loading until failure This approach is supported by previous research, as (Ferrier, 2011; Lange & Naujoks, 2006; Le-Nguyen et al., 2013), which has similarly utilized monotonic loading to investigate shear wall behavior. The experimental data were meticulously recorded through a data logger system. The cantilever structural wall specimens were categorized into two primary groups, each characterized by different aspect ratios (1.5 and 2.0). Within each group, the initial CSW specimen was reinforced using conventional reinforcement

Fig. 1 Dimension of specimens

techniques, serving as a control specimen, as depicted in Figs. 2a and 3a. Each reinforced concrete (RC) wall comprises three key components: the head beam, responsible for uniformly transferring vertical and lateral loads into the second main part, the wall panel representing the resistance shear wall, and the footing used to anchor the specimens onto a robust steel frame securely fixed to the laboratory floor. All original RC walls share identical geometric dimensions and reinforcement patterns for both the head beam and footing. The head beam features a square cross-section measuring 300×300 mm, incorporating six 12-mm-diameter deformed bars as longitudinal reinforcement. Additionally, stirrups, composed of deformed bars with a diameter of 10 mm and spaced at 155-mm intervals, contribute to the structural integrity. Similarly, the footing possesses a cross-section measuring 400×400 mm, with eight 16-mm-diameter deformed bars serving as longitudinal reinforcement. Stirrups, comprised deformed bars with a diameter of 12 mm and spaced at 150-mm intervals, further enhance the overall stability of the structure. The wall panel dimensions are as follows: length (l_w) of 1000 mm, thickness (t_w) of 150 mm, and height (h_w) of 1850 mm for the first group and 1350 mm for the second group. Concrete cover measurements are set at 20 mm for the short sides and 50 mm for the long sides.

Distinct wall web reinforcement configurations were employed for each specimen. In the case of specimens (G1-RW1-A2) and (G2-RW1-A1.5), the web was reinforced with two layers of deformed steel bars. The longitudinal reinforcement consisted of 12-mm-diameter bars, while the transfer shear reinforcement utilized 10-mm-diameter deformed steel bars. The spacing between these bars was maintained at 185 mm. For specimens (G1-RW2-A2) and (G2-RW2-A1.5), the wall web is divided into two main parts: vertical boundary elements located at the extreme right and left fibers, and the inner wall web. Each boundary element features a square cross-section measuring 150×200 mm, incorporating four 12-mm-diameter deformed bars as longitudinal reinforcement. Stirrups, composed of smooth bars with a diameter of 8 mm and spaced at 185-mm intervals, contribute to structural integrity.

The inner wall web is reinforced with two longitudinal reinforcement bars of 12 mm each, and deformed steel bars with a diameter of 10 mm and spacing of 185 mm are employed as transfer shear reinforcement.

Similarly, specimens (G1-RW3-A2) and (G2-RW3-A1.5) share the same reinforcement details as specimens (G1-RW2-A2) and (G2-RW2-A1.5), with an additional feature. They include distributed inclined reversed six bars per side, measuring 10 mm in diameter, along the
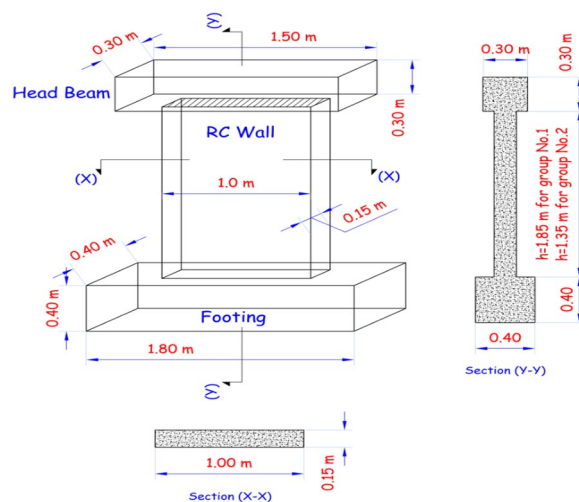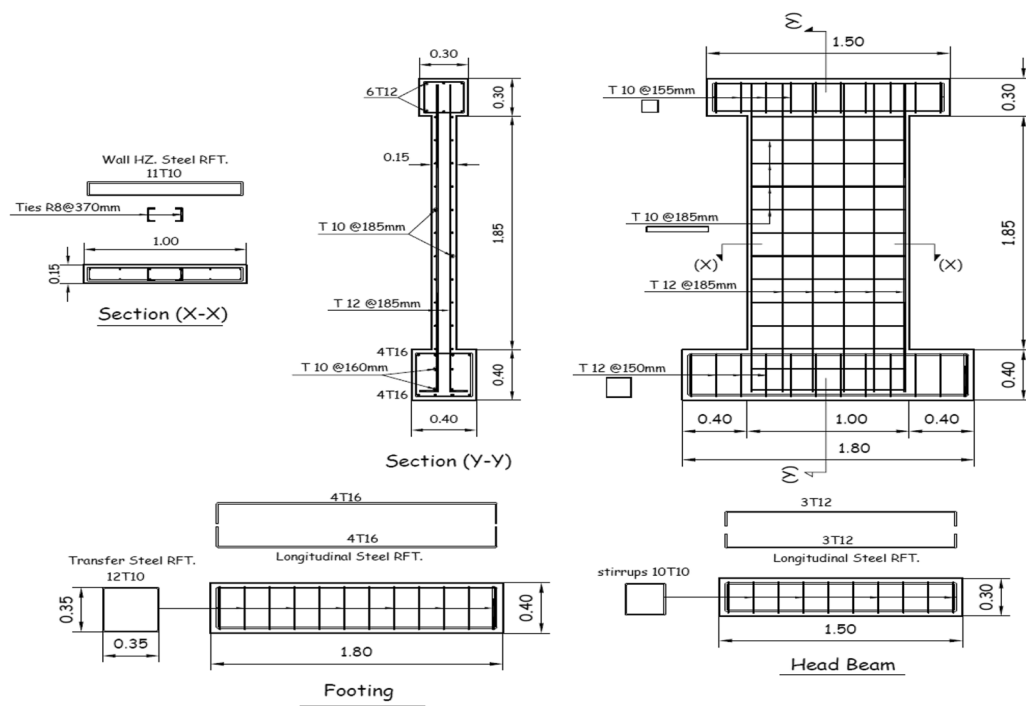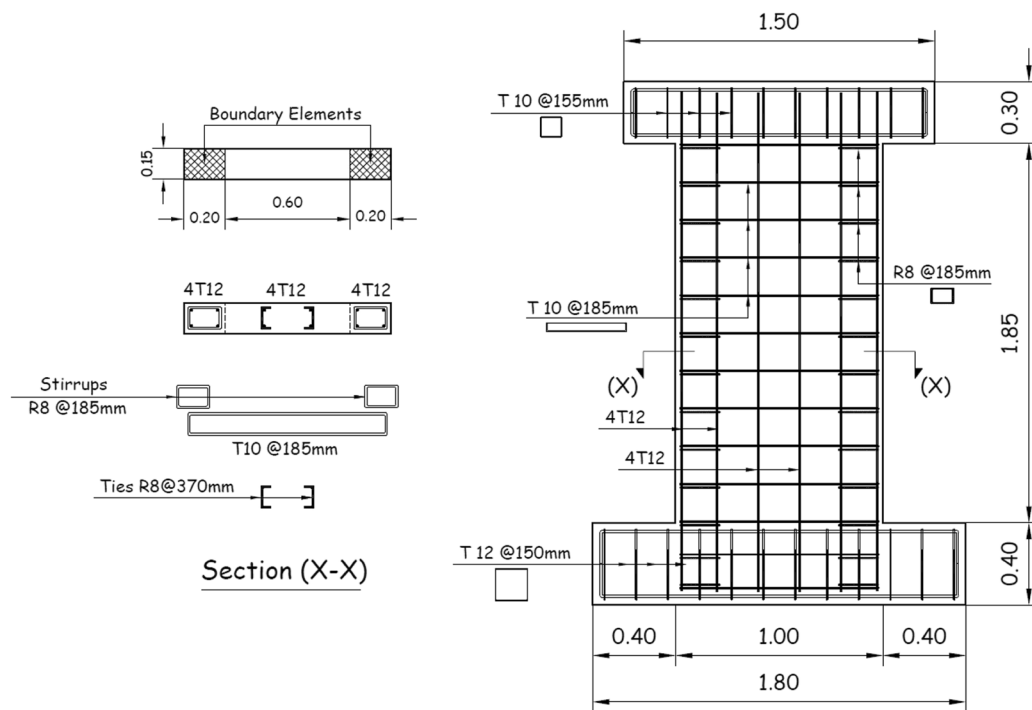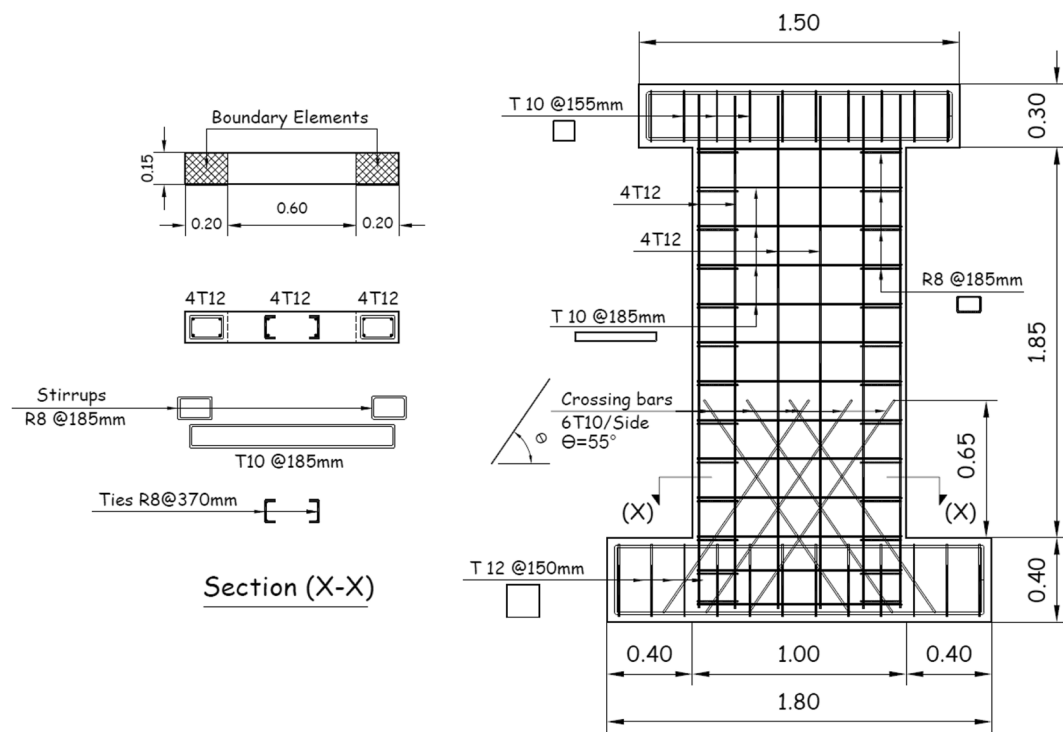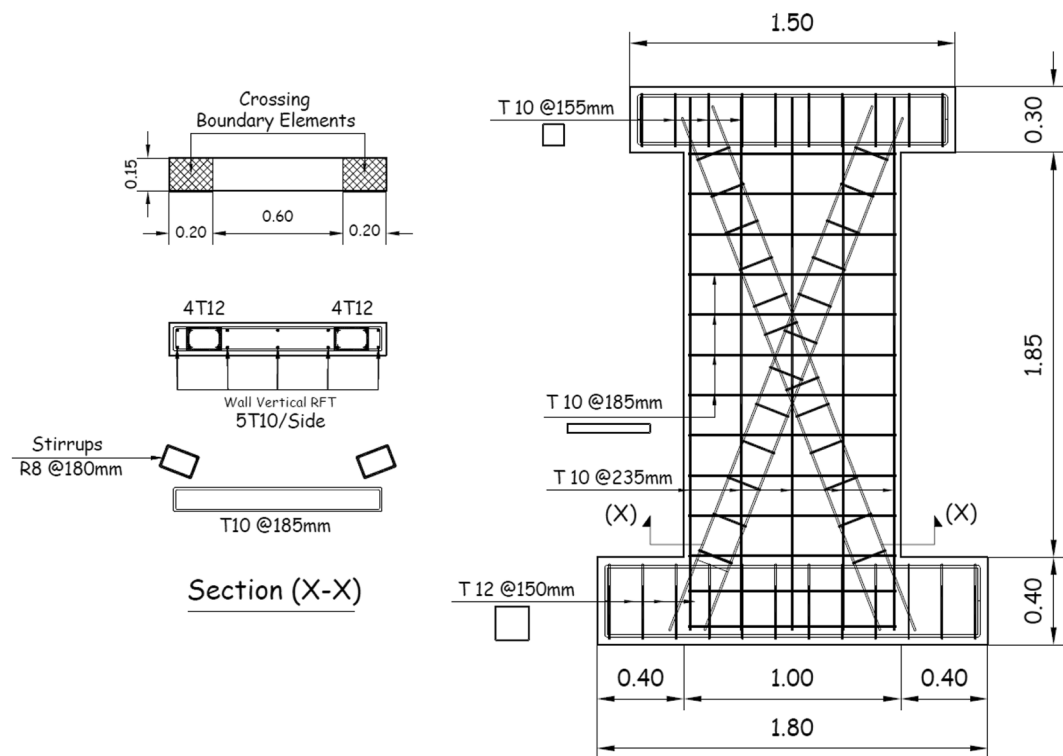
(a) G1-RW1-A2.0

(b) G1-RW2-A2.0

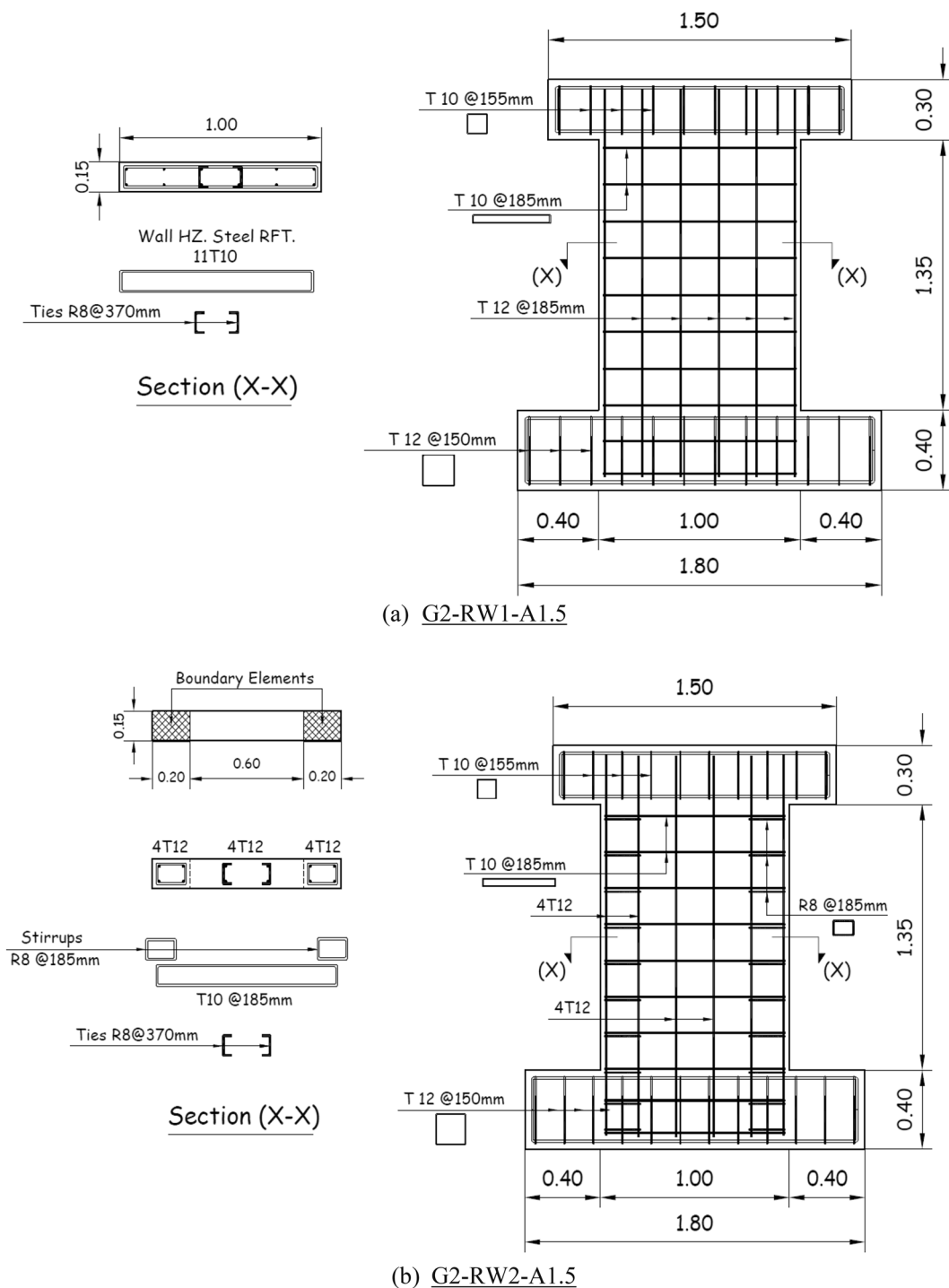**Fig. 2** Sectional dimensions and reinforcement details for Group No.1 specimens (unit: meters)

(c) G1-RW3-A2.0

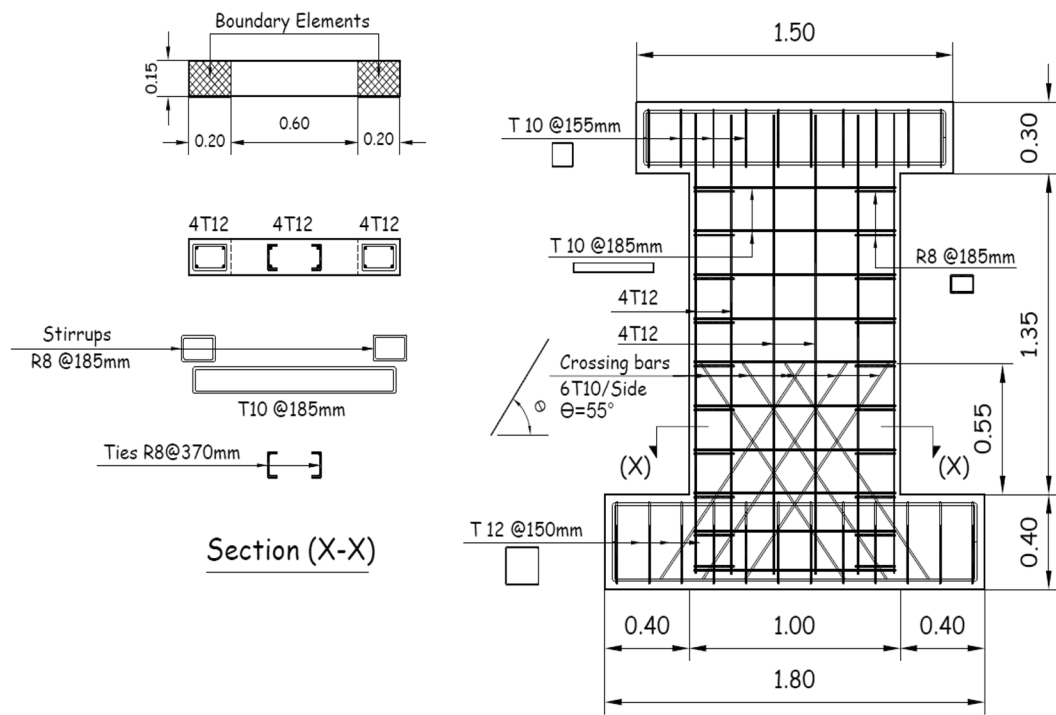(d) G1-RW4-A2.0

Fig. 2 continued

Yahia *et al. Int J Concr Struct Mater*   (2025) 19:24

Page 6 of 24

(a) G2-RW1-A1.5

(b) G2-RW2-A1.5

Fig. 3 Sectional dimensions and reinforcement details for Group No.2 specimens (unit: meters)

wall length at the first one-third of the wall height from the footing side.

For specimens (G1-RW4-A2) and (G2-RW4-A1.5), the web is reinforced with two layers of deformed steel bars. Longitudinal reinforcement consists of 10-mm-diameter bars with a spacing of 235 mm, while transfer shear reinforcement employs 10-mm-diameter deformed steel bars with a spacing of 185 mm. Additionally, an inclined embedded column with a square cross-section of 150×200 mm is incorporated. This

(c) G2-RW3-A1.5

(d) G2-RW4-A1.5

Fig. 3 continued

Table 1 Test specimens

Specimens ID		Steel reinforcement configuration									
		Web vertical steel RFT		Web horizontal steel RFT		Vertical boundary element RFT			Inclined boundary element RFT		
Group		(ρ_{vs} %)	(L_{vs})	(ρ_{hs} %)	(L_{hs})	(ρ_{bs}%)	LR_{be}	(S_{be})	(ρ_{bs}%)	LR_{be}	(S_{be})
Group No.1 Aspect ratio = 2	G1-RW1-A2.0	0.90	Φ12@185mm	0.56	Φ10@185mm	——	——	——	——	——	——
	G1-RW2-A2.0	1.0	4Φ12	0.56	Φ10@185mm	1.5	4Φ12	Φ8@185mm	——	——	——
	G1-RW3-A2.0	1.0	4Φ12	0.53	Φ10@185mm	1.5	4Φ12	Φ8@185mm	Inclined mesh 6Φ10/side	——	——
	G1-RW4-A2.0	0.52	Φ10@235mm	0.53	Φ10@185mm	——	——	——	1.5	4Φ12	Φ8@185mm
Group No.2 Aspect ratio = 1.5	G2-RW1-A1.5	0.90	Φ12@185mm	0.56	Φ10@185mm	——	——	——	——	——	——
	G2-RW2-A1.5	1.0	4Φ12	0.56	Φ10@185mm	1.5	4Φ12	Φ8@185mm	——	——	——
	G2-RW3-A1.5	1.0	4Φ12	0.56	Φ10@185mm	1.5	4Φ12	Φ8@185mm	Inclined mesh 6Φ10/side	——	——
	G2-RW4-A1.5	0.52	Φ10@235mm	0.56	Φ10@185mm	——	——	——	1.5	4Φ12	Φ8@185mm

ρ_{vs}: vertical reinforcement ratio; L_{vs}: vertical reinforcement layout; ρ_{hs}: horizontal reinforcement ratio; L_{hs}: horizontal reinforcement layout; ρ_{bs}: inclined rebars reinforcement ratio; L_{bs}: inclined rebars layout; LR_{be}: longitudinal reinforcement of boundary elements; ρ_{bs}: longitudinal steel reinforcement ratio of inclined boundary element; Sbe: stirrups of boundary elements

Yahia *et al. Int J Concr Struct Mater*   (2025) 19:24

Page 9 of 24

column features four 12-mm-diameter deformed bars as longitudinal reinforcement, and stirrups made of smooth bars with a diameter of 8 mm spaced at 185-mm intervals. The ratios of horizontal and vertical web reinforcement in each wall, denoted as ρ_{vs} and ρ_{hs}, respectively, achieved the minimum steel reinforcement requirement of 0.0025 stipulated by ACI 318−19. Furthermore, ρ_{bs} the ratio of longitudinal boundary elements steel reinforcement bars. Detailed design parameters are provided in Table 1.

2.2 Material properties

In order to validate the mechanical properties of concrete specimens, a total of six cylinders and six cubes were cast. The dimensions for the cylinders were (150 mm diameter×300 mm height), while the cubes measured (150×150×150 mm). Concrete compression testing was conducted following the guidelines of ACI 318−19 and ECP 203−17 after curing for 7 and 28 days at the Laboratory of Testing and Resistance of Materials, Faculty of Engineering, Menoufia University.

Both cylinders and cubes were subjected to testing at each time point, and the average strength was calculated. At the 28th day of curing, the average compressive strength $(f_c^{'})$ of the concrete reached 35.0 MPa. To assess the modulus of rupture of concrete (f_r), a splitting test was conducted on cylinders, and the results were compared with Eq. (1) outlined in ACI 318−19, where:

$$f_r = 0.62\sqrt{f_c^{'}}\frac{N}{mm^2}. \tag{1}$$

The examined and calculated values for concrete tensile strength were 4.0 MPa and 3.66 MPa, respectively.

For the reinforcing steel bars, tension tests were individually performed on three specimens using a universal testing machine to determine the yield strength (σy) and ultimate strength (σu). The results for 6-, 10-, 12-, and 16-mm steel bars are summarized in Table 2. The elastic modulus (*Es*) and Poisson's ratio (ν) are specified as 200 GPa and 0.2, respectively. Fig. 4 illustrates the stress–strain curve for the tested steel bars.

2.3 Experimental Setup

2.3.1 Manufacturing Processes of Test Specimens

The production of test specimens involved several stages, including shuttering preparation, steel reinforcement setup, and the installation of strain gauges, as illustrated in Fig. 5 (a to h). This process included the deployment of LVDT and the placement of strain gauges on vertical, horizontal, and inclined steel bars to measure the strain distribution.

2.3.2 Test Setup

Wall specimens were tested at the Laboratory of Reinforced Concrete, Tanta University. The testing involved vertical monotonically increasing lateral loading, treated as a horizontal load based on the specimen's setup style, until failure. A loading frame with a maximum capacity of 1000 kN was utilized for the experiments. The walls were securely fixed to the frame using rigid steel angles and plates, anchored to frame columns with 20-mm-diameter anchors. Additionally, a fixation load of 700 kN was applied to the footing to enhance its fixation to the frame and anchors.

Before testing, all reinforced concrete (RC) walls were painted silver color to facilitate crack observation. Deflections were measured at the mid-point of the head beam and at the top fixation point of the footing to the frame column, employing a Linear Variable Displacement Transducer (LVDT) to monitor specimen overturning during testing. The load was applied using a universal testing machine, and during each load increment, the load was maintained constant until a crack was observed and marked. Deflections and strains corresponding to each load increment were recorded using a data logger system.

Various parameters such as load, deflection, crack pattern, failure mode, resilience, toughness, and ductility were discussed. The loading continued until failure, and measurements were taken at all stages of loading. The static test setup details and associated instrumentation are illustrated in Fig. 6

2.4 Experimental Results and Discussion

2.4.1 Load–Displacement Response

The load–displacement behavior of all specimens was similar. In the initial load stage, no cracks were observed on the surface of tested specimens for the specimens were still in the elastic stage. With the increase of the lateral loading, horizontal cracks gradually appeared at the bottom part of specimens and some cracks developed longer and wider. Meanwhile, there were some diagonal cracks appearing on the surface of the tested shear walls for some specimens. For specimens (RW1 and RW2) in each group at higher load levels little new horizontal cracks were found at the bottom of the shear wall and the previous developed cracks longer and wider. For specimens (RW3 and RW4) in each group at higher load levels a lot new horizontal cracks were found at the bottom of the shear wall and new cracks connected between the previous developed cracks in addition to the previous developed cracks longer and wider. With the increase of the displacement, the horizontal and diagonal

Yahia *et al. Int J Concr Struct Mater*   (2025) 19:24

Page 10 of 24

Table 2 Mechanical properties of steel reinforcement bars

Reinforcement bar diameter, mm	Type	Yield strength σy, MPa	Failure strength σu, MPa
8	Plain	320	403
10	deformed	530	646
12	deformed	428	518
16	deformed	468	611
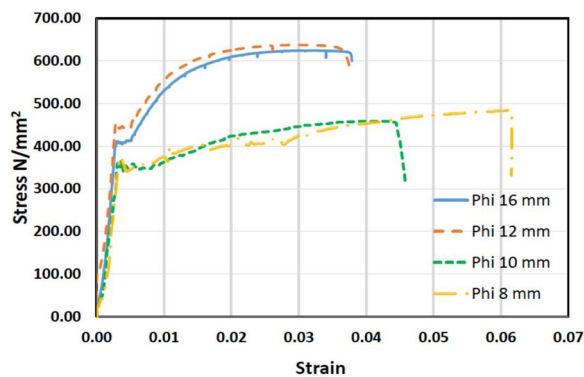
Fig. 4 Stress–strain curve for tested steel RFT bars

cracks developed quickly. In later stages of loading the concrete around the bottom of specimens began to crush and peeled off. After reaching the maximum lateral loading value, the lateral load-carrying capacity of tested specimens decreased and specimens finally reached the failure mode. The cracks on the surface of specimens reinforced with inclined rebars and steel meshing in each group developed more slowly than specimens without inclined rebars. Specimens (RW4) for each group cracks developed more horizontal than other tested specimens. All tested specimens failed due to flexural shear cracks in a ductile mode of failure. The load–displacement responses of tested specimens are similar to those depicted in Figs. 7 and 8 for each group.

2.4.2 Crack Patterns
Figure 9 depicts the progression of cracks in all specimens during both the yield and failure states. During the yield state, the yielding of the outermost longitudinal rebar is noted, while the failure state corresponds to the observed pattern at the conclusion of testing. It is noteworthy that all tested specimens failed due to flexural shear cracks in a ductile manner. Table 3 summarizes the test results for the specimens, including data on the first crack load, yield load, and peak load.

2.5 2.5. Numerical Analysis
2.5.1 Compressive Strength of Concrete Modeling
In addition to the experimental investigation numerical model had been conducted on the tested reinforced concrete structural shear walls, and results were validated by comparing the performance with the respective experimental results. For validation purposes, a three-dimensional (3D) FEM was developed to predict the behavior of the tested walls using the nonlinear finite element ABAQUS/Standard software (Abaqus & CAE, xxxx), ABAQUS standard solver method was used in this study. Concrete exhibits nonlinear behavior, transitioning from elastic to plastic characteristics after reaching the cracking stress. In the elastic stage, ABAQUS utilizes parameters such as Young's modulus (Ec) and the Poisson's ratio (υ) to define concrete behavior. The Poisson's ratio for concrete typically falls within the range of 0.15 to 0.22, with a value of 0.20. For this study. During the inelastic behavior phase, the concrete damage plasticity (CDP) model is employed. Properly defining CDP involves utilizing various commands. The key command is the damage plasticity command, which outlines five plastic damage parameters. The specific values for the concrete damage plasticity parameters used in this study are presented in Table 4. Figure 10 presents the concrete compressive behavior.

2.5.2 Tensile strength of concrete
To define the tensile stress–strain curve in the model, the tensile behavior command was used (Azam, 2015). Concrete experiences tensile cracking under uni-axial tension, the failure stress corresponds to the onset of micro-cracking in the concrete material; however, beyond the failure stress, the formation of micro-cracks is represented macroscopically with the softening stress–strain response. The following equations used to drive the stress–strain curve:

$$\sigma_t = E_{co}\varepsilon_t \; for \; \varepsilon_t \leq \varepsilon_{cr}$$

$$\sigma_t = f_t^{'}\left(\frac{\varepsilon_{cr}}{\varepsilon_t}\right)^{0.4} \; for \; \varepsilon_t > \varepsilon_{cr,}$$

Where: $\varepsilon_{cr} = \frac{f_c^{'}}{E_{co}} \; E_{co} = 5000\sqrt{f_c^{'}} \; f_t^{'} = 0.33\sqrt{f_c^{'}}$

where: E_{co} the initial modulus of elasticity, ε_t the concrete tensile strain, $f_t^{'}$ the tensile strength of concrete (peak stress), and ε_{cr} the concrete strain at peak stress (at cracking).

2.5.3 Element Selection
The C3D8R element and the T3D2 element were utilized to simulate the concrete and reinforcements, respectively,
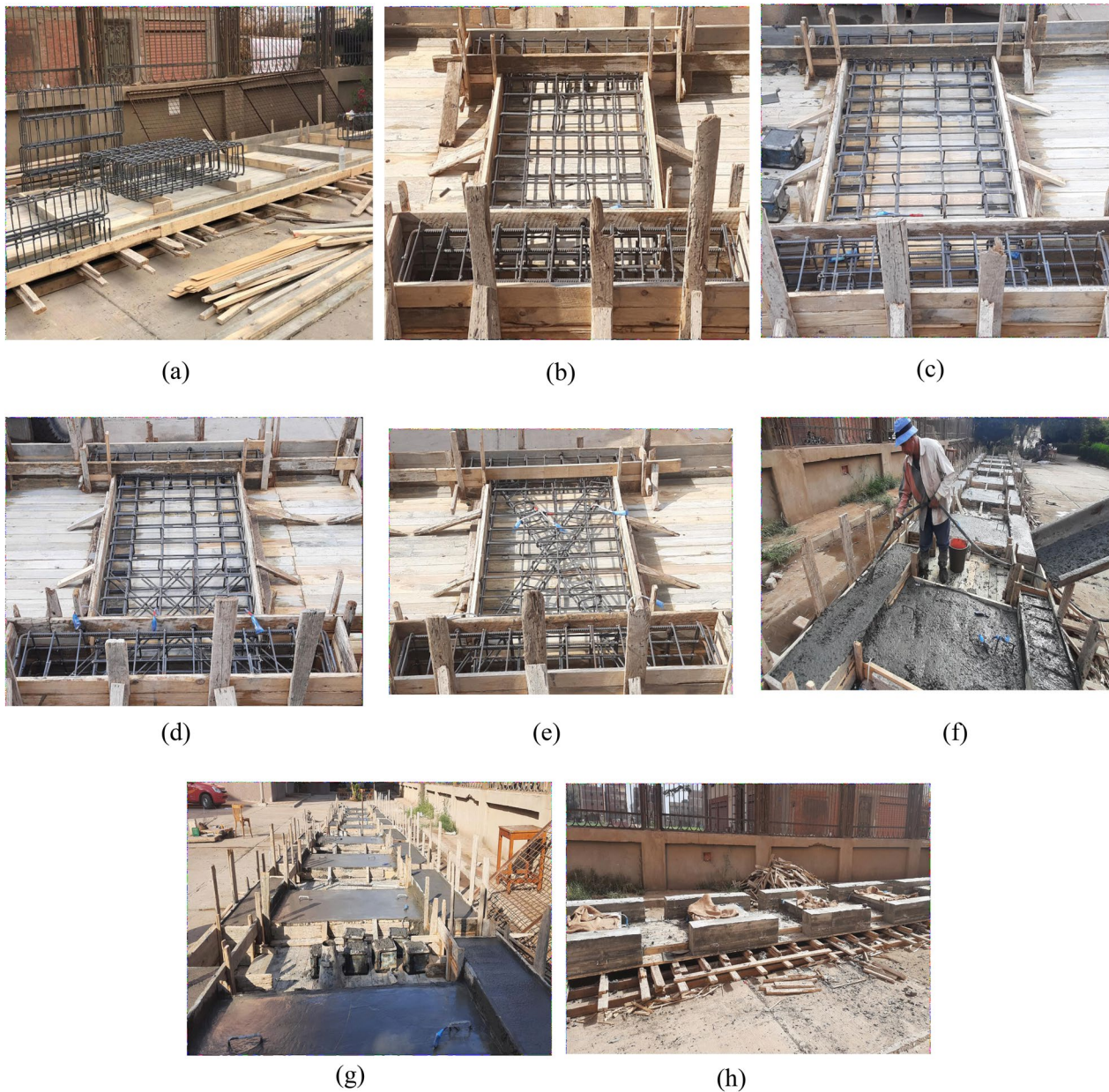
Fig. 5 Walls manufacturing process. **a** Shuttering preparation. **b** Ordinary wall (G2-RW1-A1.5). **c** Wall with vertical boundary elements (G2-RW2-A1.5). **d** Wall with vertical boundary element and mesh (G2-RW3-A1.5). **e** Wall with inclined embedded column (G2-RW4-A1.5). **f** Concrete casting. **g** Preparing of concrete surface. **h** Shuttering removal after curing

in this study. To ensure the validity of the concrete damage plasticity (CDP) specimen, a model validation was conducted in two steps. In the first step, the model was verified by comparing the load–deflection behavior with the experimental results of the control beam. A parametric study was performed for evaluating a suitable dilation angle and mesh size for the FE model. The verification dilation angles for concrete were 30°, 32° and 35°. The mesh sensitivity analysis started from a coarse mesh to very fine meshes. The mesh element sizes for concrete were 60 mm, 50 mm and 40 mm. The results show that C3D8R elements with dilation angles ranging from 30° to 32° and with mesh sizes ranging from 40 to 50 mm is more suitable for specimens modeling.

In the second step, the load–deflection behavior of each specimen was compared between the finite element (FE) model predictions and the experimental results.
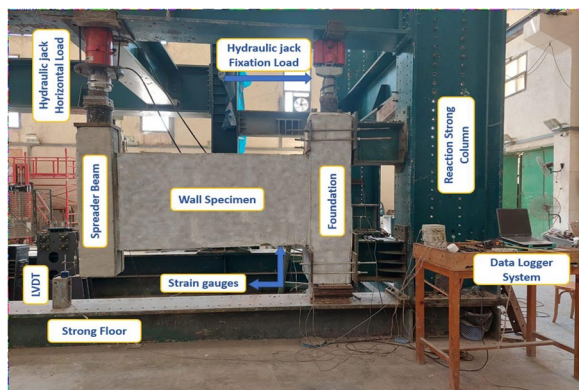
Yahia *et al. Int J Concr Struct Mater*   (2025) 19:24

Page 12 of 24

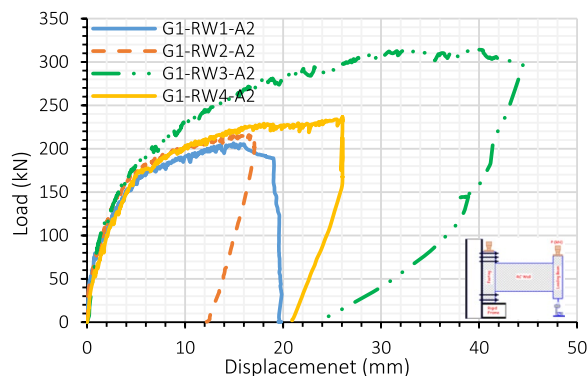**Fig. 6** Test setup for a typical wall specimen

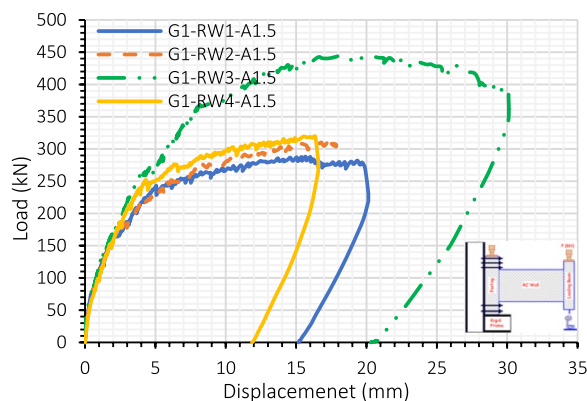**Fig. 7** Load–displacement curve for group No.1 specimens

Fig. 8 Load–displacement curve for group No.2 specimens

Figures 11 and 12 illustrate the model validation concerning dilation angle and meshing size, respectively.

2.5.4 Assembly of Sketched Elements
In the assembly module, each element was individually sketched and subsequently merged using the available constraint options. These constraint options were also

employed to align the reinforcement in the same direction as the concrete beam and to translate instances, ensuring they were appropriately positioned, as illustrated in Fig. 13.

2.5.5 Element Contact
The introduction of "Constraints" was essential for assessing the real behavior of wall responses concerning the reinforcing materials employed. Through the utilization of the "embedded region" function, the reinforcing materials were effectively constrained within the concrete element. This function establishes a host region for concrete beams, depicted in Fig. 14. By employing this constraint, it becomes possible to assume a flawless bond between the concrete and all reinforcing materials. Alternatively, the contact surfaces between the concrete segments of the wall were assembled and linked together using tie-constraints as shown in Fig. 15. These constraints ensure that specified surfaces or regions remain in contact throughout the analysis, allowing for accurate representation of interactions, such as frictionless contact, sliding, or adherence (Abaqus & CAE, xxxx).

2.5.6 Load Application and Boundary Conditions
Boundary conditions are essential for achieving accurate results in finite element simulations. In this particular case, the footing of the wall model was replicated in ABAQUS as a fixed base. Furthermore, the load was incrementally applied in the lateral direction to each wall model to mimic the experimental conditions. Figures 16 and 17 depict the boundary conditions and load application in the ABAQUS model, respectively.

2.6 Results and discussion
Figures 18 and 19 present a comparison of concrete failure patterns between the finite element (FE) analysis and experimental results for the typical four specimens. It is evident that the damage state of each specimen can be effectively simulated using the concrete constitutive relationship models established in this study. Figure 20 displays the stress of the steel reinforcement bars at the point of failure. Additionally, Fig. 21 illustrates the comparison of load–displacement behavior between the experimental and FE analysis results. Furthermore, Tables 5, 6, 7 provide a comparison between experimental and FE model data regarding the first crack load, yield load, and peak load for all tested specimens and their corresponding FE models.

It can be seen that the load–displacement curves developed by the FE model fitted well with the experimental
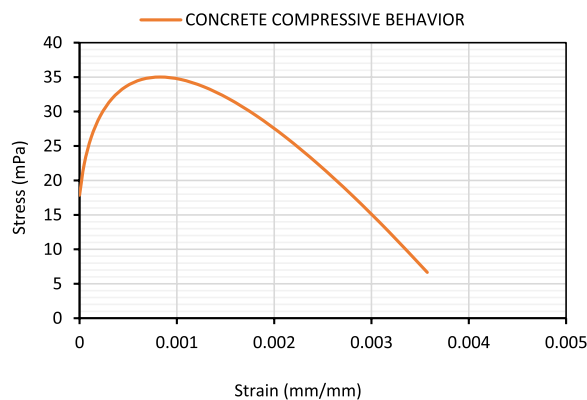
(a) G1-RW1-A2.0

(b) G1-RW2-A2.0

(c) G1-RW3-A2.0

(d) G1-RW4-A2.0

(e) G2-RW1-A1.5

(f) G2-RW2-A1.5

(g) G2-RW3-A1.5

(h) G2-RW4-A1.5

Fig. 9 Specimens crack distribution

Table 3 Summary of experimental results

Test No	Group aspect ratio	Specimen ID	Cracking load		Yielding load		Peak load	
			Load (kN)	Deflection (mm)	Load (kN)	Deflection (mm)	Load (kN)	Deflection (mm)
1	2	G1-RW1-A2.0	39.24	0.222	131.29	2.96	206.39	14.93
2		G1-RW2-A2.0	50.49	0.376	126.99	2.35	217.26	16.35
3		G1-RW3-A2.0	51.51	0.619	198.9	6.54	314.16	39.88
4		G1-RW4-A2.0	67.83	1.09	172.38	6.75	236.64	26.06
5	1.5	G2-RW1-A1.5	73.95	0.53	193.8	3.276	288.15	15.65
6		G2-RW2-A1.5	73.44	0.484	182.58	2.53	310.59	17.26
7		G2-RW3-A1.5	89.25	0.66	256.53	3.83	445.23	18.42
8		G2-RW4-A1.5	80.07	0.68	250.92	4.36	319.33	16.36

Table 4 Concrete damage plasticity parameters for M-350

Dilation angle (ψ)	**32**
Flow potential eccentricity (∈)	0.1
Biaxial/uniaxial compression plastic strain ratio ($\sigma b0/ \sigma c0$)	1.16
Invariant stress ratio **Kc**	0.6667
Viscosity (μ)	0.005

Fig. 10 Concrete compressive behavior

Fig. 11 Validation of dilation angle
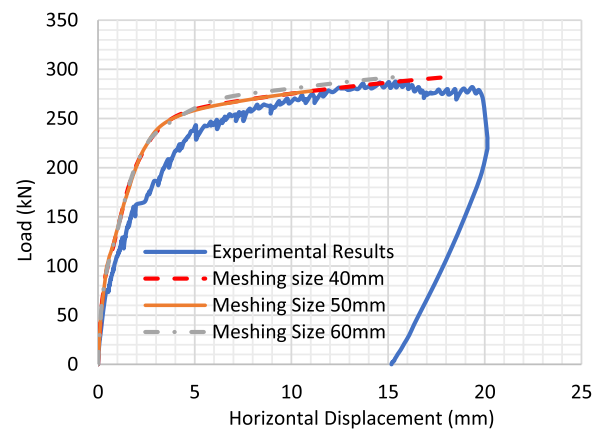
**Fig. 12** Validation of mesh size

curves, and the simulated characteristic points were in good agreement with the test characteristic points, especially the characteristic loads. For the characteristic load of each specimen, the error between the simulated and experimental values was mostly controlled within 20% at cracking, yielding stage and 6% at failure stage. For the characteristic displacement of each specimen, the error between the simulated and experimental values was mostly controlled within 70% at cracking, yielding stage and 20% at failure stage, It should be noted that the main reason large error in displacement obtained from FE set to be completely tied with the simulation and experimental results is that the bottom surface of foundations was bottom surface of specimens in FE simulation; while actually specimens did not reach this ideal state.
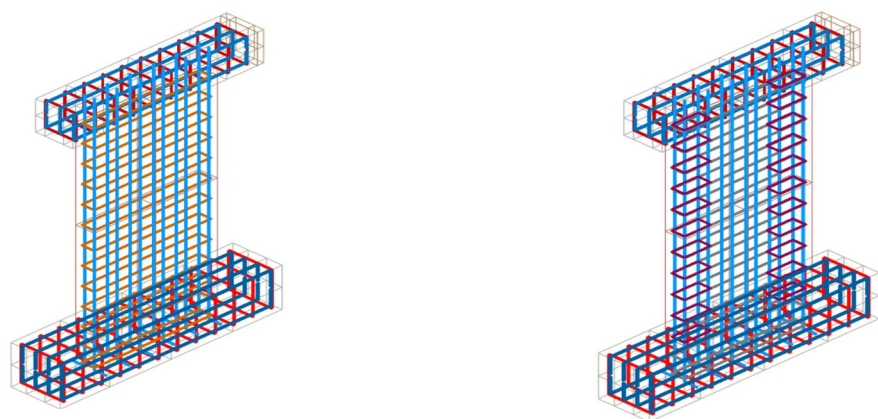
(a) Assembly of cantilever structural wall (RW1) elements

(b) Assembly of cantilever structural wall (RW2) elements
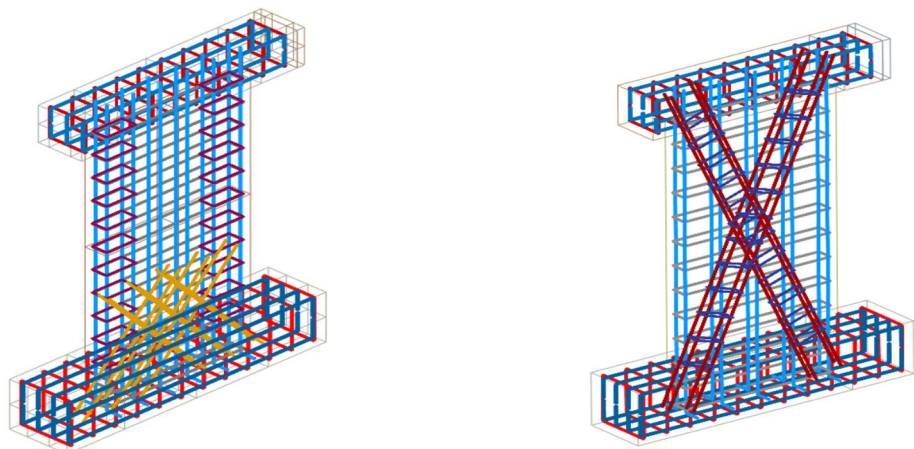
(c) Assembly of cantilever structural wall (RW3) elements

(d) Assembly of cantilever structural wall (RW4) elements

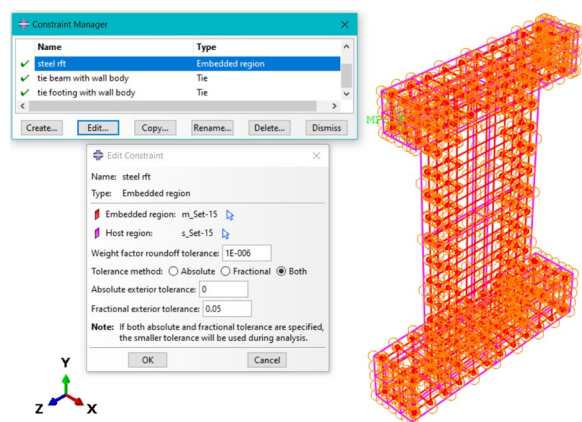**Fig. 13** Assembly of cantilever structural walls with different steel reinforcement configurations

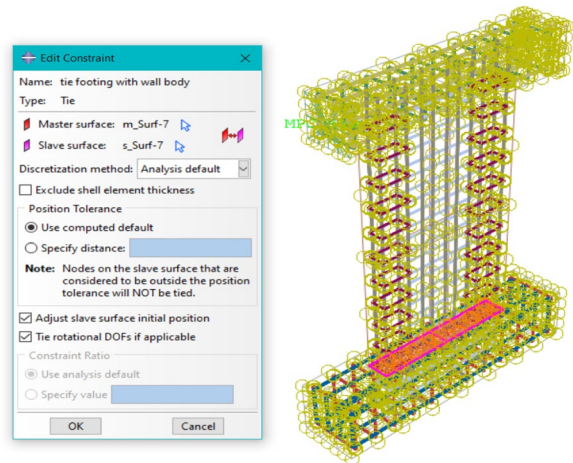**Fig. 14** Contact between host concrete element and steel reinforcement bars

Fig. 15 Tie contact between concrete elements

Yahia *et al. Int J Concr Struct Mater*   (2025) 19:24
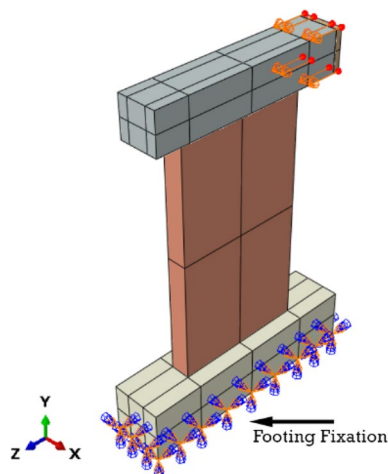
Page 16 of 24

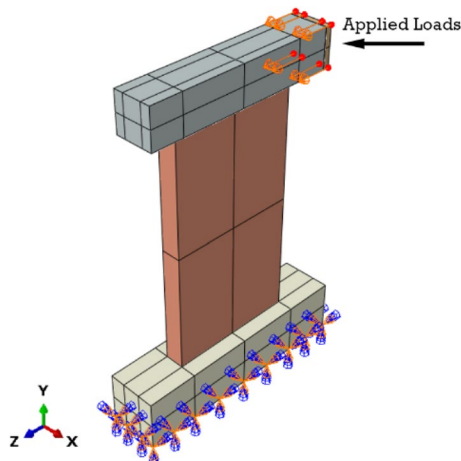**Fig. 16** The boundary conditions of the (CSW)

Fig. 17 Applying lateral forces

2.6.1 Effect of Using Different Steel Reinforcement Configuration on Walls Capacity

Different steel reinforcement configurations were used to study the effect on the flexural behavior of reinforced concrete shear walls in three terms cracking, yielding and peak loads. Results of tested specimens for each group were compared with specimen (RW-1) as control specimen. For group No.1 with aspect ratio of 2.0, specimens (RW2, RW3 and RW4) exhibit an increase in cracking load of (28.66%, 31.26% and 72.86%), respectively. For yielding loads, specimen (RW2) exhibits a decrease of 27.7%, for specimens (RW3 and RW4) exhibit an increase of (51.44% and 31.3%), respectively. For peak loads specimens (RW2, RW3 and RW4) exhibit an increase in peak load of (5.27%, 52.21% and 14.65%), respectively. For

group No.2 with aspect ratio of 1.5, specimens (RW2, RW3 and RW4) exhibit an increase in cracking load of (0.1%, 20.69% and 8.3%), respectively. For yielding loads, specimen (RW2) exhibits a decrease of 5.78%, for specimens (RW3 and RW4) exhibit an increase of (32.37% and 29.4%), respectively. For peak loads specimens (RW2, RW3 and RW4) exhibit an increase in peak load of (7.79%, 54.51% and 10.8%), respectively. Table 8 presents effect of using different steel reinforcement configurations on cracking, yielding and peak loads for each tested group.

2.6.1.1 Effect of Using Various Steel Reinforcement Configuration on Ductility   Evaluating the ductility of reinforced concrete walls (RCW) holds significant importance. Ductility, in this context, refers to the ability of the structure to endure inelastic deformation without a loss in its load-carrying capacity prior to failure. The measure of ductility deformation can be expressed in terms of deflection. Table 9 provides the ductility index and initial stiffness for the tested specimens. The results indicated that the reinforcing of concrete wall with different steel configurations has a significant impact on ductility. For the first group with aspect ratio of 2.0, specimen (G1-RW2-A2.0) exhibits the maximum increase in deflection ductility index of 39% with respect to specimen (G1-RW1-A2.0). For the second group with aspect ratio of 1.5, specimen (G2-RW2-A1.5) exhibit the maximum increase in deflection ductility index of 41.7% with respect to specimen (G2-RW1-A1.5). So, reinforcing with vertical boundary columns only has the maximum ductility for concrete walls. In addition, concrete walls with high aspect ratio values have more ductile response.

2.6.1.2 Effect of Using Various Steel Reinforcement Configuration on Resilience and Toughness   Toughness is the energy absorbed to fracture while resilience is the energy absorbed to yield load. For the first group with aspect ratio of 2.0, specimen (G1-RW2-A2.0) exhibits the maximum increase in resilience of 442.0% with respect to specimen (G1-RW1-A2.0). For the second group with aspect ratio of 1.5, specimen (G2-RW4-A1.5) exhibits the maximum increase in resilience of 57.0% with respect to specimen (G2-RW1-A1.5). For the first group with aspect ratio of 2.0, specimen (G1-RW3-A2.0) exhibits the maximum increase in toughness of 331.2% with respect to specimen (G1-RW1-A2.0). For the second group with aspect ratio of 1.5, specimen (G2-RW3-A1.5) exhibits the maximum increase in toughness of 68.2% with respect to specimen (G2-RW1-A1.5). The values of resilience and toughness are presented in Table 10.

Fig. 18 Comparison of the concrete failure patterns between the FE analysis and test results in tension for Group No I. **a** Crack pattern for (G1-RW1-A2.0). **b** Crack pattern for (G1-RW2-A2.0). **c** Crack pattern for (G1-RW3-A2.0). **d** Crack Pattern for (G1-RW4-A2.0)
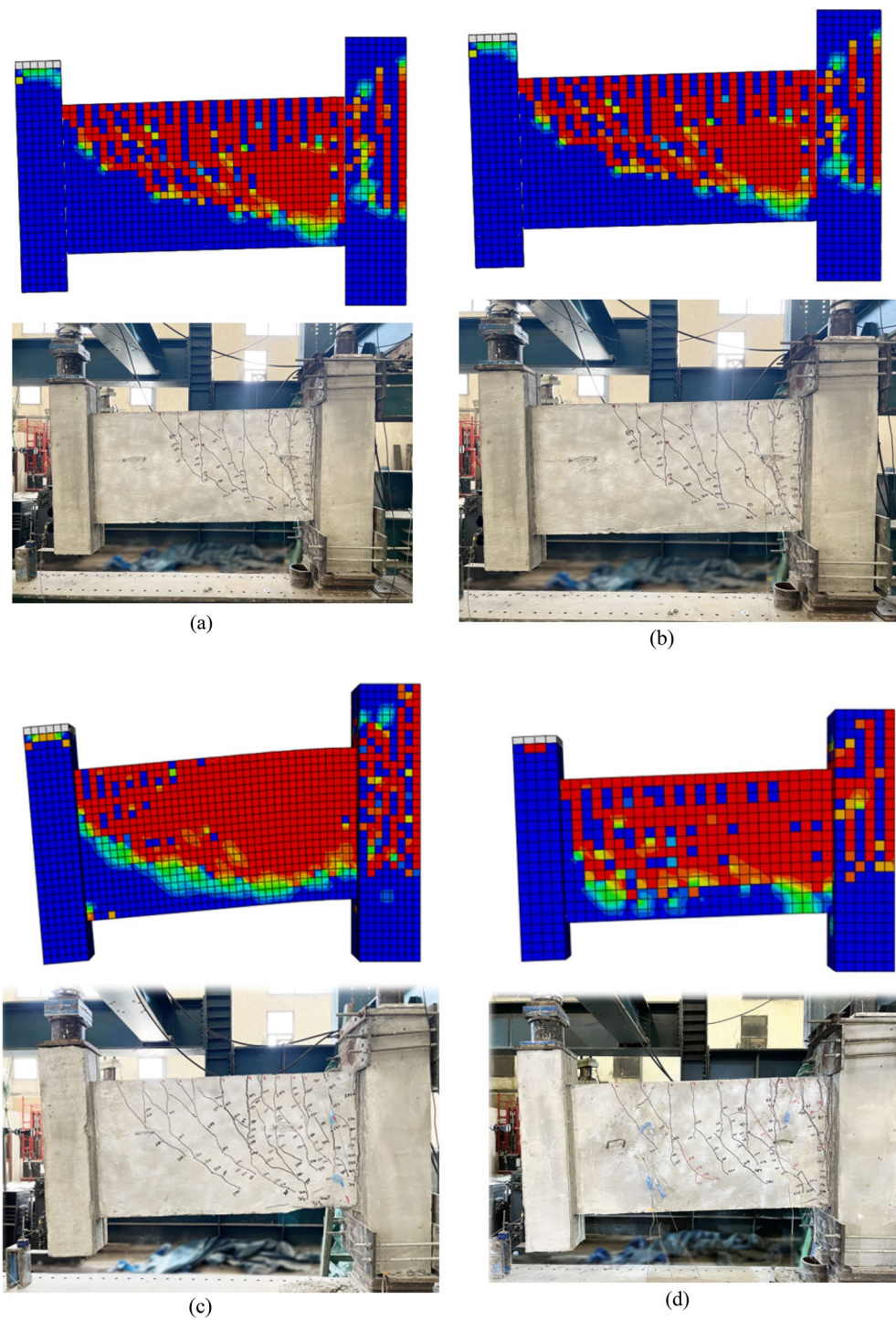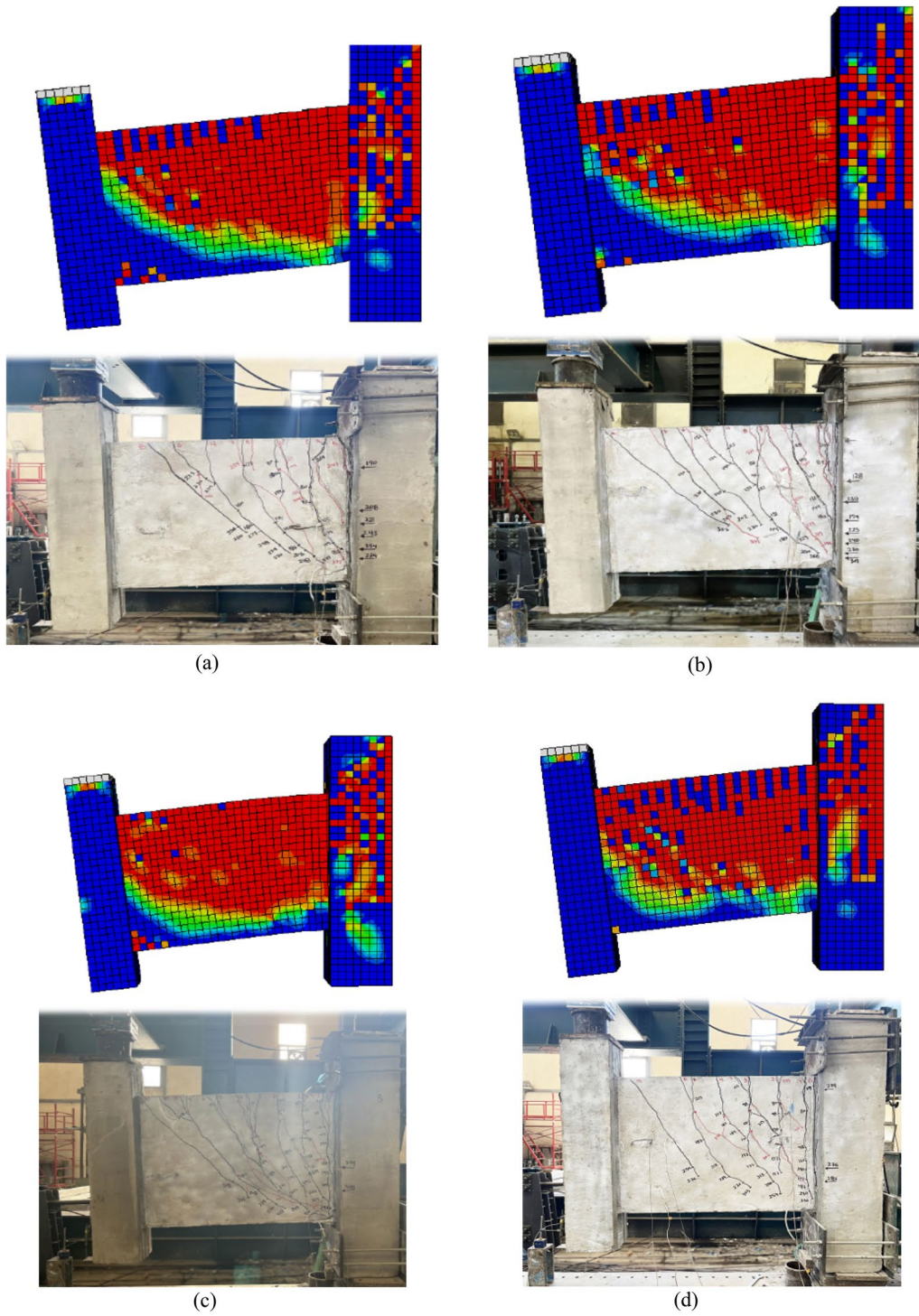
Fig. 19 Comparison of the concrete failure patterns between the FE analysis and test results in tension for Group No II. **a** Crack pattern for (G2-RW1-A1.5). **b** Crack pattern for (G2-RW2-A1.5). **c** Crack pattern for (G2-RW3-A1.5). **d** Crack pattern for (G2-RW4-A1.5)
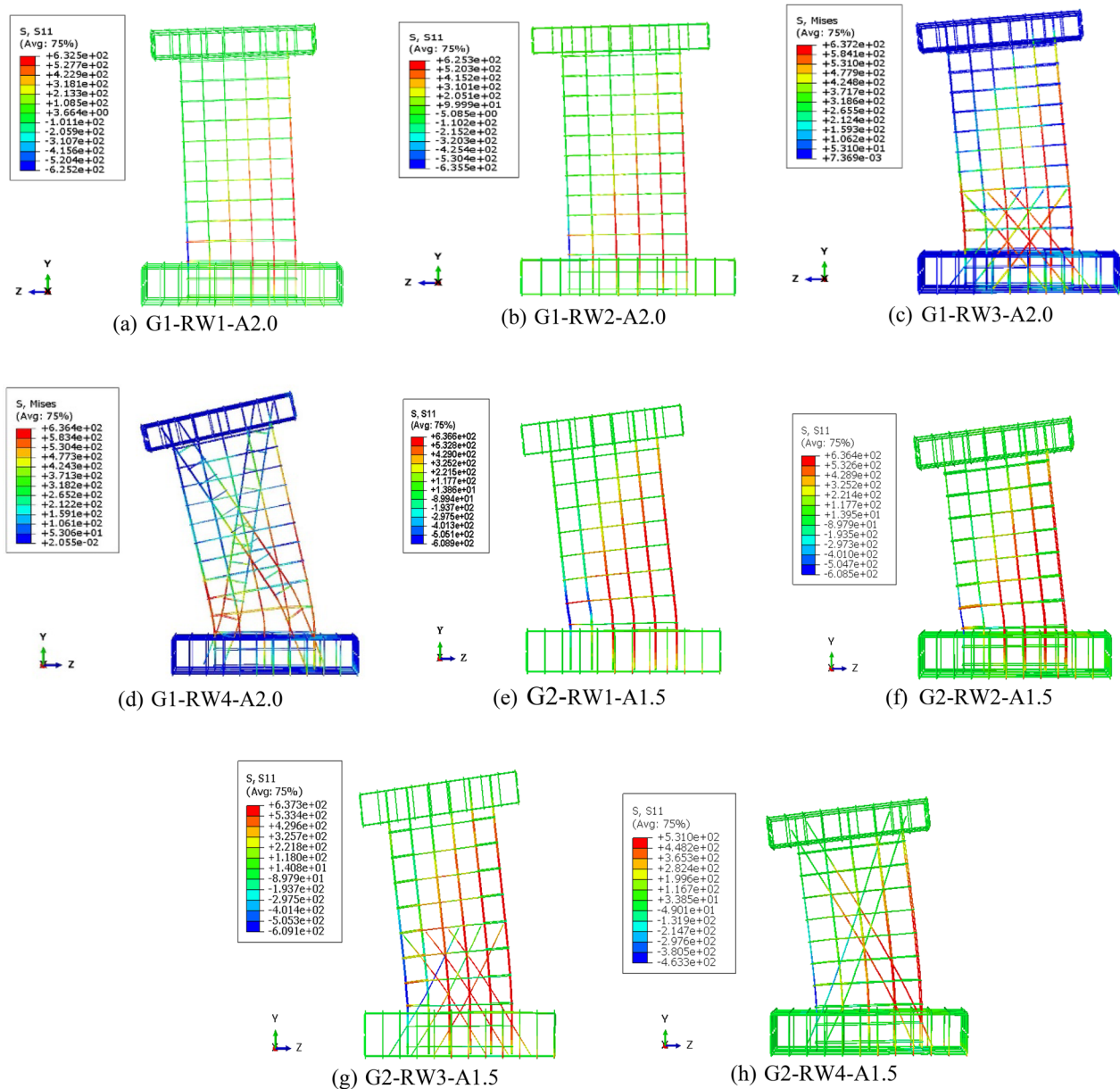
(a) G1-RW1-A2.0   (b) G1-RW2-A2.0   (c) G1-RW3-A2.0

(d) G1-RW4-A2.0   (e) G2-RW1-A1.5   (f) G2-RW2-A1.5

(g) G2-RW3-A1.5   (h) G2-RW4-A1.5

Fig. 20 Stress of the steel reinforcement bars at failure state for group No I and II

3 Conclusions

Eight large-scale cantilever structural wall (CSW) specimens with different steel reinforcement configuration, were tested under monotonically increasing lateral loading up to failure and results recorded by using data logger system. Based on the test results and the finite element analysis model of different kinds of shear walls were established and verified. The following conclusions can be drawn:

1. The load-carrying capacity at cracking, yielding, and peak points of concrete structural walls was significantly improved through various steel reinforcement configurations. By adding embedded vertical columns at the boundary elements, including both vertical columns with a diagonal mesh at the lower part of the walls, and diagonal embedded columns, the capacity increased by 72.86%, 51.44%, and 52.21% for group 1, and by 20.69%, 32.37%, and 54.51% for group 2, respectively.
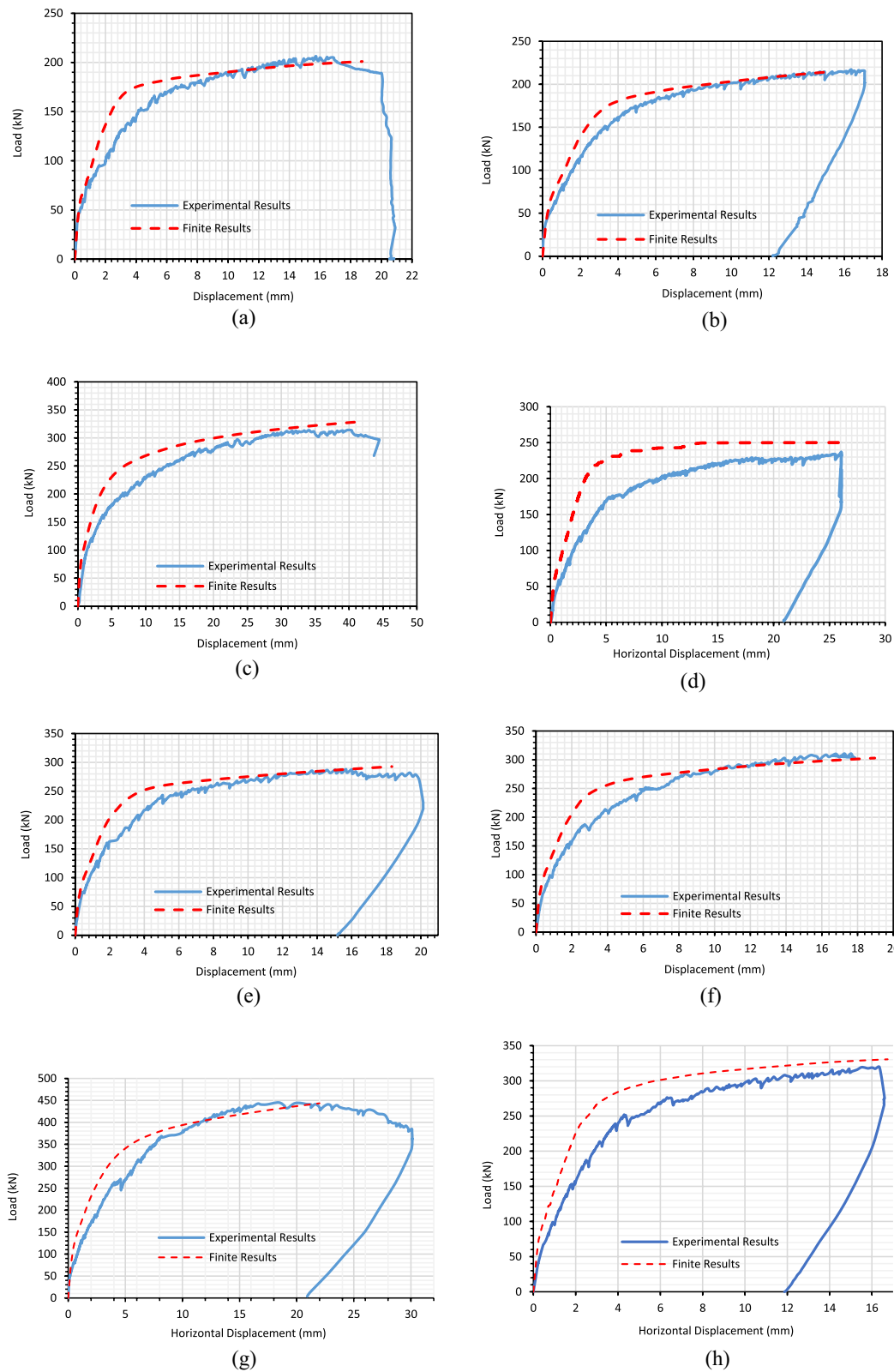
Fig. 21 Comparison of load–displacement curve between experimental and finite element results. Load–displacement curve for (G1-RW1-A2.0). **a** Load–displacement curve for (G1-RW2-A2.0). **b** Load–displacement curve for (G1-RW3-A2.0). **c** Load–displacement curve for (G1-RW4-A2.0). **d** Load–displacement curve for (G2-RW1-A1.5).**e** Load–displacement curve for (G2-RW2-A1.5). **f** Load–displacement curve for (G2-RW3-A1.5). **g** Load–displacement curve for (G2-RW4-A1.5)

Yahia *et al. Int J Concr Struct Mater*   (2025) 19:24

Page 21 of 24

Table 5 Experimental and finite element analysis first crack loads

Test No	Group aspect ratio	Specimen ID	Cracking stage results					
			Experimental results		Finite results		The percentage of variances	
			Load (kN)	Deflection (mm)	Load (kN)	Deflection (mm)	$\Delta P\%$	$\Delta\delta\%$
1	Group No.1 AR = 2.0	G1-RW1-A2.0	39.24	0.22	44.89	0.23	14.4	4.54
2		G1-RW2-A2.0	50.49	0.376	51.4	0.279	1.8	25.8
3		G1-RW3-A2.0	51.51	0.619	58.6	0.296	13.8	52.1
4		G1-RW4-A2.0	67.83	1.09	53.4	0.313	21.8	71.2
5	Group No.2 AR = 1.5	G2-RW1-A1.5	73.95	0.53	65.17	0.217	11.1	59.0
6		G2-RW2-A1.5	73.44	0.484	66.78	0.214	9.0	55.8
7		G2-RW3-A1.5	89.25	0.66	78.44	0.256	12.1	61.2
8		G2-RW4-A1.5	80.07	0.68	74.33	0.25	21.8	21.8

Table 6 Experimental and finite element analysis first yield loads

Test No	Group aspect ratio	Specimen ID	Yield stage results					
			Experimental results		Finite results		The percentage of variances	
			Load (kN)	Deflection (mm)	Load (kN)	Deflection (mm)	$\Delta P\%$	$\Delta\delta\%$
1	Group No.1 AR = 2.0	G1-RW1-A2.0	131.29	2.96	148.58	2.35	13.2	20.6
2		G1-RW2-A2.0	126.99	2.35	113.26	1.41	19.4	40.0
3		G1-RW3-A2.0	198.9	6.54	215.84	4.1	8.5	37.3
4		G1-RW4-A2.0	172.38	6.75	168.9	2.39	1.4	64.5
5	Group No.2 AR = 1.5	G2-RW1-A1.5	193.8	3.276	208.17	2.12	7.4	35.2
6		G2-RW2-A1.5	182.58	2.53	204.03	1.97	11.7	22.1
7		G2-RW3-A1.5	256.53	3.83	260.65	2.55	1.6	33.4
8		G2-RW4-A1.5	250.92	4.36	244.2	2.34	3.5	21.8

Table 7 Experimental and finite element analysis first peak loads

Test No	Group aspect ratio	Specimen ID	peak stage results					
			Experimental results		Finite results		The percentage of variances	
			Load (kN)	Deflection (mm)	Load (kN)	Deflection (mm)	$\Delta P\%$	$\Delta\delta\%$
1	Group No.1 AR = 2.0	G1-RW1-A2.0	206.39	14.93	200.27	17.84	3.0	19.4
2		G1-RW2-A2.0	217.26	16.35	214.07	14.91	1.46	8.8
3		G1-RW3-A2.0	314.16	39.88	329.47	42.23	4.8	5.9
4		G1-RW4-A2.0	236.64	26.06	250.0	26.26	5.6	0.77
5	Group No.2 AR = 1.5	G2-RW1-A1.5	288.15	15.65	292.73	18.32	1.6	17.0
6		G2-RW2-A1.5	310.59	17.26	302.88	18.96	2.5	9.8
7		G2-RW3-A1.5	445.23	18.42	443.34	21.99	0.4	19.4
8		G2-RW4-A1.5	319.33	16.36	330.63	16.75	3.5	2.4

Yahia *et al. Int J Concr Struct Mater*   (2025) 19:24

Page 22 of 24

Table 8 Effect of using different steel reinforcement configurations on cracking, yielding and peak loads for each tested group

| Test No | Group aspect ratio | Specimen ID | Experimental results | | | | | |
| | | | Initial cracking loads | | Yielding loads | | Peak loads | |
			Load (kN)	Δ_{cr}%	Load (kN)	Δ_y%	Load (kN)	Δ_p%
1	Group No.1 AR = 2.0	G1-RW1-A2.0	39.24	–	131.29	–	206.39	–
2		G1-RW2-A2.0	50.49	28.66	126.99	-3.27	217.26	5.27
3		G1-RW3-A2.0	51.51	31.26	198.9	51.44	314.16	52.21
4		G1-RW4-A2.0	67.83	72.86	172.38	31.3	236.64	14.65
5	Group No.2 AR = 1.5	G2-RW1-A1.5	73.95	–	193.8	–	288.15	–
6		G2-RW2-A1.5	73.44	0.1	182.58	-5.78	310.59	7.79
7		G2-RW3-A1.5	89.25	20.69	256.53	32.37	445.23	54.51
8		G2-RW4-A1.5	80.07	8.3	250.92	29.4	319.33	10.8

Table 9 Ductility index and initial stiffness of tested (RCW)

Group ID	Wall specimen	Ductility index	Ductility increasing rate %	Initial stiffness, (kN/mm)
Group No.1	G1-RW1-A2.0	5.0	–	176.75
	G1-RW2-A2.0	6.95	39.0	134.28
	G1-RW3-A2.0	6.1	22	83.2
	G1-RW4-A2.0	3.86	-22.8	62.22
Group No.2	G2-RW1-A1.5	4.8	–	138.5
	G2-RW2-A1.5	6.8	41.67	151.73
	G2-RW3-A1.5	4.8	0	135.22
	G2-RW4-A1.5	3.75	-21.9	117.75

2. Both reinforcement strategies—adding embedded vertical columns at the boundary elements with a diagonal mesh at the lower part of the walls, and using diagonal embedded columns—effectively restrained crack development and reduced crack widths. The diagonal steel mesh, in particular, had a more significant impact in mitigating wall damage.

3. The embedded diagonal columns in shear walls convert a portion of lateral forces into axial forces (either tensile or compressive, depending on the loading direction). This conversion helps manage the forces more efficiently, reducing the generation of large moments on the walls.

4. In Group 1, specimens G1-RW2-A2.0 and G1-RW3-A2.0 showed significant increases in ductility, by 128% and 22%, respectively, while specimen G1-RW4-A2.0 experienced a 22.8% decrease in ductility compared to the control specimen G1-RW1-A2.0. In Group 2, specimen G2-RW2-A1.5 displayed

Table 10 Resilience and toughness values

Group ID	Wall specimen	Resilience kN.m	$\Delta_{Resilience}$%	Toughness kN.m	$\Delta_{Toughness}$%
Group No.1 Aspect ratio = 2.0	G1-RW1-A2.0	267.1	–	2444.82	–
	G1-RW2-A2.0	1447.59	442	2888.55	18.2
	G1-RW3-A2.0	967.35	262	10,541.88	331
	G1-RW4-A2.0	596.0	123	4654.64	90.4
Group No.2 Aspect ratio = 1.5	G2-RW1-A1.5	426.17	–	3669.2	–
	G2-RW2-A1.5	296.13	-30.51	4456.88	21.46
	G2-RW3-A1.5	611.3	43.44	6172.62	68.22
	G2-RW4-A1.5	669.25	57.0	4105.58	11.89

a 41.7% increase in ductility, whereas G2-RW3-A1.5 showed no improvement, and G2-RW4-A1.5 had a 21.8% decrease in ductility relative to the control specimen G2-RW1-A1.5. These results indicate that specimens with an aspect ratio of 2.0 generally exhibit superior ductility compared to those with an aspect ratio of 1.5, suggesting that higher aspect ratios may be more suitable for high seismic zones.

5. The use of different steel reinforcement configurations significantly enhances resilience and toughness, with increases of up to 442% and 331% respectively for Group No.1 with an aspect ratio of 2.0 and increases of 57% and 45.5% for Group No.2 with an aspect ratio of 1.5. Specimens with an aspect ratio of 2.0 exhibit a greater effect on increasing resilience and toughness compared to those with an aspect ratio of 1.5.

6. When employing different steel reinforcement configurations, reinforcing concrete walls using the RW3 technique in each group with aspect ratios of 1.5 and 2.0 showed the maximum increase in peak loads of 52.71% and 54.51% respectively compared to control specimens.

7. Similarly, reinforcing concrete walls using the RW2 reinforcement technique in each group with aspect ratios of 1.5 and 2.0 exhibited the maximum increase in ductility of 128% and 41.7%, respectively, compared to control specimens.

Declarations

Competing interests

References

ABAQUS. Abaqus/CAE User's Manual. Dassault Systems Simulia Corp, Providence; Rl: USA.

Azam, A. (2015), 'Numerical Modelling of Reinforced Concrete Walls Encased in Polyvinyl Chloride Stay-in-place Formwork'

ACI Committee 318 (2019), Building Code Requirements for Structural Concrete (ACI 318–19), American Concrete Institute.

de Barros Silva, J. R., Horowitz, B., & Bernardo, L. F. A. (2023). Nonlinear analysis of planar H-Shaped and U-Shaped Thin Reinforced Concrete Shear Walls. *Structures, 49*, 295–311.

Du, K., Luo, H., & Sun, J. (2020). Cyclic testing of moment-shear force interaction in reinforced concrete shear wall substructures. *Earthquake Eng Eng Vibration, 19*(2), 465–481.

Egyptian code of practice, Design and construction for reinforced concrete structures, ECP 203–2020.

Ferrier, E. (2011). Mechanical Behaviour of Concrete Walls Under Static Loading.

Hasan, M., Qasem, M., & Muhamad, R. (2023). Finite element modeling of precast reinforced concrete wall with dual boundary elements under lateral load. *Materials Today*. https://doi.org/10.1016/j.matpr.2023.03.688

Hosseini, S. M., Yekrangnia, M., & Vatani Oskouei, A. (2022). Effect of spiral transverse bars on structural behavior of concrete shear walls reinforced with GFRP bars. *J Building Eng*. https://doi.org/10.1016/j.jobe.2022.104706

Hu, R., Fang, Z., & Benmokrane, B. (2023). Nonlinear finite-element analysis for predicting the cyclic behavior of UHPC shear walls reinforced with FRP and steel bars. *Structures, 53*, 265–278.

Huang, Z., et al. (2020). Shear behavior of concrete shear walls with CFRP grids under lateral cyclic loading. *Engineering Struct*. https://doi.org/10.1016/j.engstruct.2020.110422

Lange, J., & Naujoks, B. (2006). Behaviour of cold-formed steel shear walls under horizontal and vertical loads. *Thin-Walled Struct, 44*, 1214–1222.

Le-Nguyen, Khuong, Brun, Michael, Limam, Ali, Ferrier, E., & Michel, Laurent. (2013). Local and Non-Local Approaches for Simulating CFRP-Reinforced Concrete Shear Walls Under Monotonic Loads.

Li, H.-N., Tang, Y.-C., Li, C., & Wang, L.-M. (2019). Experimental and numerical investigations on seismic behavior of hybrid braced precast concrete shear walls. *Engineering Structures*. https://doi.org/10.1016/j.engstruct.2019.109560

Li, X., et al. (2022). Seismic behavior of steel fiber reinforced high strength concrete shear walls with different embedded steel configurations. *J Building Eng*. https://doi.org/10.1016/j.jobe.2022.104551

Li, X., et al. (2023). The effects of steel fibers and boundary elements on the seismic behavior of high-strength concrete shear walls. *J Building Eng*. https://doi.org/10.1016/j.jobe.2023.106415

Nagib, M. T., et al. (2022). Interfacial shear behavior between UHPFRC layers and normal concrete substrate for shear-strengthened squat RC shear walls under cyclic loading. *Engineering Structures*. https://doi.org/10.1016/j.engstruct.2022.113850

Ren, F., et al. (2022). Lateral force-resisting behavior of GFRP-tube reinforced concrete-filled multicellular steel tubular shear walls under cyclic loads. *J Building Eng*. https://doi.org/10.1016/j.jobe.2021.103541

Shen, D., Yang, Q., Jiao, Y., Cui, Z., & Zhang, J. (2017). Experimental investigations on reinforced concrete shear walls strengthened with basalt fiber-reinforced polymers under cyclic load. *Construction and Building Materials, 136*, 217–229.

Wei, F., Chen, H., & Xie, Y. (2022). Experimental study on seismic behavior of reinforced concrete shear walls with low shear span ratio. *J Building Eng*. https://doi.org/10.1016/j.jobe.2021.103602

Xing, Y., et al. (2022). Seismic behavior of steel truss and concrete composite shear wall with double X-shaped braces. *J Building Eng*. https://doi.org/10.1016/j.jobe.2022.105399

Zhang, J. W., et al. (2019). Seismic Behavior of Low-rise Concrete Shear Wall with Single Layer of Web Reinforcement and Inclined Rebars: Restoring Force Model. *KSCE J Civil Eng, 23*(3), 1302–1319.

Zhang, J., et al. (2021). Seismic behavior of steel fiber-reinforced high-strength concrete mid-rise shear walls with high-strength steel rebar. *J Building Eng*. https://doi.org/10.1016/j.jobe.2021.102462

Zhao, Q., et al. (2019). Experimental investigation of shear walls using carbon fiber reinforced polymer bars under cyclic lateral loading. *Engineering Structures, 191*, 82–91.

Publisher's Note

Springer Nature remains neutral with regard to jurisdictional claims in published maps and institutional affiliations.

Ahmed Yahia is a PhD student at the Faculty of Engineering, Menoufia University, specializing in the design and construction of reinforced concrete structures. His research focuses on advancing the safety, efficiency, and sustainability of concrete structures through innovative design methodologies.

Magdy Tayel is a professor of reinforced concrete structures at the Faculty of Engineering, Menoufia University. He has authored numerous publications in the field, with a particular emphasis on earthquake engineering and the structural systems of high-rise buildings. His work aims to enhance the resilience and stability of structures under seismic conditions.

Khalid Heiza is a professor of reinforced concrete structures at the Faculty of Engineering, Menoufia University. With extensive research contributions in his field, his recent work focuses on strengthening and repairing structural elements to improve their durability and performance in both new and existing structures.

Ghada Hekal is an associate professor at the Faculty of Engineering, Menoufia University. She has published extensively on dynamic analysis, optimization, and finite element analysis of structural elements. Her research aims to improve the design and analysis techniques used to assess the behavior of complex structures under various loading conditions.